UWB Geo-Regioning using Multivariate Channel Statistics

Christoph Steiner and Armin Wittneben
Communication Technology Laboratory
ETHZ CH-8092 Zurich
Email: {steinech,wittneben}@nari.ee.ethz.ch

***Abstract*— Ultra-Wideband (UWB) Geo-Regioning is an approach to localize UWB transmitters by means of their channel impulse responses. A received channel impulse response is assigned to a geographic region based on a-priori known characteristics of this region. The first approach relying on knowledge of the average power delay profile of the channel was presented and analyzed in [1], [2], [3]. In this paper we extend this method by including the knowledge of the correlation between channel taps. We discuss this new modeling assumption, derive the respective multivariate maximum likelihood decision algorithm, provide an analytic expression for the probabilities of misclassification, and present simulation results based on measured channel impulse responses. A significant performance gain is visible compared to the previous average power delay profile approach, where the taps are assumed to be independent.**

I. Introduction

One of the most cited advantages of Ultra-Wideband (UWB) technology is the capability of performing accurate localization [4]. The huge bandwidth of the transmit signal, which is much higher than the coherence bandwidth of the channel, renders the effective channel as highly frequency selective. Thus, for a static scenario with non-moving receiver, transmitter, and scatterers, the channel can be modeled as a linear time invariant filter with many filter taps, which implies a very high temporal resolution of different multipaths including an accurate representation of the initial delay. Therefore, a lot of localization and ranging approaches in UWB are based on Time-of-Arrival (ToA) estimation [5], [6], [7], [8], where the unknown position of a transmitter is calculated using the estimated distances to 3, 4 or more reference receivers with known positions. In typical Line-of-Sight (LOS) conditions, the first path (initial delay) is also the strongest path. However, a general problem of localization, ranging, and tracking systems using ToA estimates is the performance degradation in non-LOS conditions, since here the strongest and/or first arriving path may not correspond to the direct path [6], [7].

UWB Geo-Regioning differs from the above mentioned methods in terms of goals, applications, physical background, and methodology. The idea is to assign UWB transmitters by means of their channel impulse responses (CIRs) to a-priori defined regions by exploiting the capability of high temporal resolution of multipath components due to the UWB transmit signal. The CIRs from different regions exhibit significant differences in their multipath propagation properties due to the scattering environment. This implies that UWB Geo-Regioning relies very much on a rich scattering environment. The goal is not necessarily to determine the absolute position of a transmitter up to an uncertainty of a few centimeters, but instead to be able to judge wether this transmitter is situated in a well defined geographical region and/or belongs to a well defined group of transmitters (e.g. cluster).

It would be of great advantage to have this region information in a sensor network. For example, environmental data can be linked on the fly to its geographical origin. Thinking of an ad-hoc network with many wireless nodes, the clustering of this network can be done using the region information accounting for the geometric properties of the network. Knowing these clusters is of great help for routing protocols. Besides, UWB Geo-Regioning can also aid localization systems to achieve more accurate position estimates.

The region information can be obtained by any communication system using channel estimation. Additional advantages are the robustness of UWB Geo-Regioning to non-LOS conditions and, moreover, that it does not require exact timing and synchronization. Also, it is sufficient to use a single receiver, whereas there are at least 3 distributed receivers necessary for ToA based approaches.

In this work, the existing UWB Geo-Regioning approach [1], [2], [3] based on the knowledge of the average power delay profile (APDP) of different regions is extended to a multivariate approach using the covariance matrices of these regions as characteristics. The next section describes the modeling assumptions and the estimation of the covariance matrix. In Section III, the multivariate maximum likelihood decision algorithm is derived, and its performance is analyzed in Section IV. Section V explains the simulation setup, and Section VI shows and discusses the simulation results. Section VII summarizes the contribution of the paper and gives an outlook into further work.

Notation: All vectors are column vectors, $j = \sqrt{-1}$, I is the identity matrix, $(\cdot)^T$ denotes transposition, $(\cdot)^H$ denotes conjugate complex transposition. The operator E(·) denotes the expectation operator, trace(·) is the sum of the diagonal elements of a matrix, and eig(·) calculates the eigenvalues of a matrix. The capital letters A and B denote geographic regions and conterminously the two hypotheses:

A ... CIR originates in region A.
B ... CIR originates in region B.

II. Modeling Assumptions

The discrete time samples of a complex baseband equivalent CIR are modeled as a circular symmetric, complex Gaussian random vector with covariance matrix Σ. A covariance matrix specifying region A is denoted as Σ_A. The entries on the main diagonal of Σ correspond to the APDP of this region.

The CIR samples are corrupted by additive white Gaussian noise with zero mean and variance σ^2. Thus, the probability density function (PDF) of a discrete time CIR $\vec{x} = [x[1], x[2], \ldots, x[K]]^T$ of length K samples originating in region A is given by

$$p(\vec{x}|A) = \mathcal{CN}\left(\vec{0}, \Sigma_A + \sigma^2 I\right) = \frac{1}{\pi^K |\Sigma_A + \sigma^2 I|} \exp\left(-\vec{x}^H \left(\Sigma_A + \sigma^2 I\right)^{-1} \vec{x}\right),$$

where

$$\Sigma_A = \mathrm{E}\left(\vec{x}_A \vec{x}_A^H\right).$$

The random vector $\vec{x}_A$ is a realization of the multivariate, circular symmetric, complex normal distribution.

The maximum likelihood estimator for the covariance matrix Σ_A using $N > K$ independent observations $\vec{x}_{A,1}, \vec{x}_{A,2}, \ldots, \vec{x}_{A,N}$ is given according to [9] by

$$\Sigma_A = \frac{1}{N} \sum_{i=1}^{N} \left(\vec{x}_{A,i} - \vec{0}\right) \left(\vec{x}_{A,i} - \vec{0}\right)^H.$$

The estimated covariance matrix Σ_A, serving as a statistical model for region A, is distributed according to a Wishart distribution [9].

The signal to noise ratio (SNR) in dB is defined as

$$\mathrm{SNR} = 10 \log_{10}\left(\frac{\mathrm{trace}\left(\Sigma_A\right)}{\sigma^2}\right) = 10 \log_{10}\left(\frac{\mathrm{trace}\left(\Sigma_B\right)}{\sigma^2}\right),$$

where it is assumed that the sums of the eigenvalues (traces) of two covariance matrices representing region A and B are equal. This corresponds to an energy equalization of the APDPs meaning that different receive energies due to different distances (path losses) of UWB transmitters are not taken into account for the decision process.

Fig. 1 shows the APDPs of two exemplary regions A and B, i.e., the main diagonals of the corresponding covariance matrices Σ_A and Σ_B, in an observation window of length 45 nanoseconds (ns). For a sampling time of 0.15 ns this results in a total length of 300 samples.

III. Multivariate Maximum Likelihood Decision Algorithm

According to the modeling assumptions the PDFs for the samples of the CIRs originating in regions A and B are given by

$$p(\vec{x}|A) = \mathcal{CN}\left(\vec{0}, \Sigma_A + \sigma^2 I\right)$$
$$p(\vec{x}|B) = \mathcal{CN}\left(\vec{0}, \Sigma_B + \sigma^2 I\right).$$

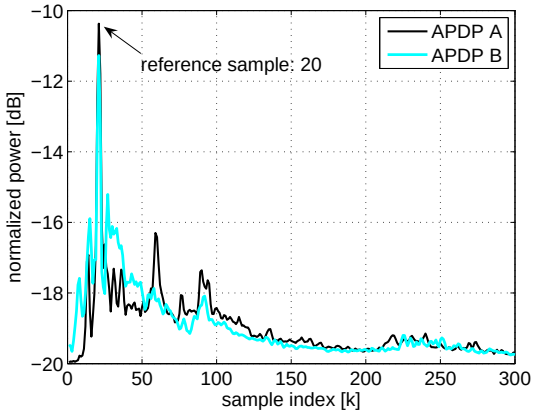

Fig. 1. APDPs for regions A and B at SNR = 20 dB.

The maximum likelihood decision between these two hypotheses with equal a-priori probabilities is given by

$$p(\vec{x}|A) \underset{B}{\overset{A}{\gtrless}} p(\vec{x}|B)$$
$$\pi^{-K} \left|\Sigma_A + \sigma^2 I\right|^{-1} \exp\left(-\vec{x}^H \left(\Sigma_A + \sigma^2 I\right)^{-1} \vec{x}\right) \underset{B}{\overset{A}{\gtrless}}$$
$$\pi^{-K} \left|\Sigma_B + \sigma^2 I\right|^{-1} \exp\left(-\vec{x}^H \left(\Sigma_B + \sigma^2 I\right)^{-1} \vec{x}\right),$$

and by simplifying this expression we get the maximum likelihood decision rule as

$$\vec{x}^H \Delta \vec{x} \underset{B}{\overset{A}{\gtrless}} \delta,$$

where the matrix $\Delta = \left(\Sigma_B + \sigma^2 I\right)^{-1} - \left(\Sigma_A + \sigma^2 I\right)^{-1}$ is Hermitian, since $\Sigma_A + \sigma^2 I$ and $\Sigma_B + \sigma^2 I$ are Hermitian and so are their inverses. The decision threshold δ is given by

$$\delta = \ln \frac{\left|\Sigma_A + \sigma^2 I\right|}{\left|\Sigma_B + \sigma^2 I\right|}.$$

In order to analyze the performance of this algorithm, analytic expressions for the two error probabilities

$$P_{e|A} = P\left(\vec{x}^H \Delta \vec{x} \leq \delta | A\right)$$
$$P_{e|B} = P\left(\vec{x}^H \Delta \vec{x} > \delta | B\right)$$

must be derived. Consequently, the PDF of the quadratic Hermitian form $\vec{x}^H \Delta \vec{x}$ is derived in Section IV. In the following, hypothesis A is considered. The derivation stays the same for hypothesis B. Nevertheless, the resulting PDFs have in general different parameters under each hypothesis, which makes the decision problem asymmetric, implying that both probabilities have to be considered.

IV. Analysis of Multivariate Maximum Likelihood Algorithm

The problem considered hereafter is to find the PDF, through its characteristic function, of a general Hermitian form given by

$$z = \vec{x}^H \Delta \vec{x}.$$

The following derivations can be found in more detail in Appendix B of [10].

A. Reduction to Diagonal Hermitian Form

The first step is to whiten the CIR vector $\vec{x}$. This is done by diagonalizing the covariance matrix $\Sigma_A + \sigma^2 I$ of $\vec{x}$ according to

$$\Sigma_A + \sigma^2 I = U_A \Lambda_A U_A^H,$$

where the real valued and nonnegative eigenvalues are stored in Λ_A, and the corresponding eigenvectors in the columns of the unitary matrix U_A. Thus, writing

$$\vec{w} = \Lambda_A^{-0.5} U_A^H \vec{x}$$

renders the random vector $\vec{w}$ with zero mean and following covariance matrix:

$$\begin{aligned} \mathrm{E}\left(\vec{w}\vec{w}^H\right) &= \Lambda_A^{-0.5} U_A^H \mathrm{E}\left(\vec{x}\vec{x}^H\right) U_A \Lambda_A^{-0.5} \\ &= \Lambda_A^{-0.5} U_A^H U_A \Lambda_A U_A^H U_A \Lambda_A^{-0.5} = I. \end{aligned}$$

With this linear transformation the general Hermitian form becomes

$$z = \vec{w}^H \Theta \vec{w},$$

where the matrix $\Theta = \Lambda_A^{0.5} U_A^H \Delta U_A \Lambda_A^{0.5}$ is again Hermitian and can be diagonalized according to

$$\Theta = V \Phi_A V^H.$$

The eigenvalues in Φ_A are real but not necessarily all positive. With one more linear transformation

$$\vec{v} = V^H \vec{w},$$

a diagonal quadratic form is obtained:

$$z = \vec{v}^H \Phi_A \vec{v} = \sum_{k=1}^{K} \phi[k] |v[k]|^2, \tag{1}$$

where the covariance matrix of $\vec{v}$ is still the identity matrix I.

Thus, the searched PDF is a weighted sum of i.i.d. exponentially distributed random variables with mean 1, or equivalently, a sum of independent, exponentially distributed random variables with means $\phi[k]$.

In general, there can exist several weights with the same values. Thus, the characteristic function of a diagonal quadratic form, assuming positive weights, is given by

$$\Psi(j\omega) = \prod_{i=1}^{N} \left(\frac{1}{1 - j\omega\phi[i]} \right)^{N_i} \prod_{k=1+NN_i}^{K} \left(\frac{1}{1 - j\omega\phi[k]} \right),$$

where there are $K - NN_i$ mutually distinct weights and N weights with multiplicity N_i. For all weights mutually distinct ($N = 0$) or all equal ($N = 1$ and $N_i = K$), the PDF for z is expressed in closed form in [11]. For one weight ($N = 1$) with multiplicity N_1 and $K - N_1$ mutually distinct weights, a closed form expression for z can be found in [12]. To the best of the authors' knowledge, no closed form expression is known for the general case. For the derivation of the error probabilities in the next section, it is assumed that all weights are mutually different. It has been observed that the weights obtained from the measurement data (cf. Section V) are in fact distinct, although some differ only after the 4-th position after the decimal point causing numerical instabilities in MatLab. However, these weights are always below 10^{-1} in absolute value (cf. Fig. 2), and thus, do not contribute much to the error probabilities. Therefore, the calculated error probabilities are good approximations to the real ones, which is also shown in Section VI.

B. Analytic Probabilities of Misclassification

The weights (cf. Fig. 2) under hypothesis A are given by

$$\begin{aligned} \vec{\phi}_A = [\phi_A[1], \phi_A[2], \ldots, \phi_A[K]]^T = \\ \mathrm{eig}\left(\Lambda_A^{0.5} U_A^H \Delta U_A \Lambda_A^{0.5}\right). \end{aligned}$$

and under hypothesis B by

$$\begin{aligned} \vec{\phi}_B = [\phi_B[1], \phi_B[2], \ldots, \phi_B[K]]^T = \\ \mathrm{eig}\left(\Lambda_B^{0.5} U_B^H \Delta U_B \Lambda_B^{0.5}\right). \end{aligned}$$

Fig. 2 depicts two exemplary weighting vectors $\vec{\phi}_A$ and $\vec{\phi}_B$,

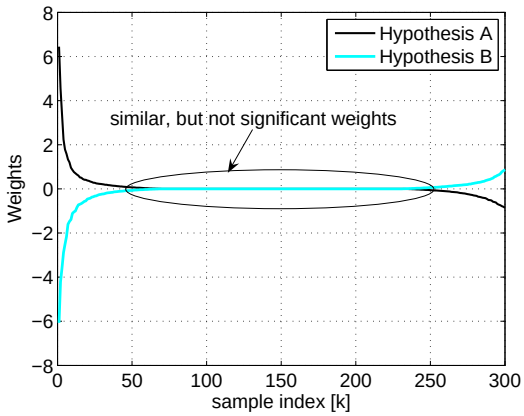

Fig. 2. Weights $\vec{\phi}_A$ and $\vec{\phi}_B$ at SNR = 20 dB

where most of the weights ($\approx$ two-thirds) are below 10^{-1} and do not contribute significantly to the error probability.

Since the weights can be positive or negative, the sum in (1) is split into a part collecting all positive and a part collecting all negative weights according to

$$\begin{aligned} z_1 &= \sum_{k_1=1}^{K_1} |\phi[k_1]||v[k_1]|^2 \quad \text{for } \phi[k_1] > 0 \\ z_2 &= \sum_{k_2=K_1+1}^{K} |\phi[k_2]||v[k_2]|^2 \quad \text{for } \phi[k_2] \leq 0 \\ z &= z_1 - z_2, \end{aligned}$$

with independent random variables z_1 and z_2.

The PDFs of z_1 and z_2 under hypothesis A are given by (cf. [11])

$$f_{z_1|A}(z) = \sum_{k_1=1}^{K_1} \frac{C_{1|A}[k_1]}{\phi_A[k_1]} \exp\left(-\frac{z}{\phi_A[k_1]}\right)$$
$$f_{z_2|A}(z) = \sum_{k_2=K_1+1}^{K} \frac{C_{2|A}[k_2]}{\phi_A[k_2]} \exp\left(-\frac{z}{\phi_A[k_2]}\right),$$

where

$$C_{1|A}[k_1] = \prod_{i=1 \ i\neq k_1}^{K_1} \frac{\phi_A[k_1]}{\phi_A[k_1]-\phi_A[i]}$$
$$C_{2|A}[k_2] = \prod_{i=K_1+1 \ i\neq k_2}^{K} \frac{\phi_A[k_2]}{\phi_A[k_2]-\phi_A[i]}.$$

Thus, the probability of misclassification $P_{e|A}$ under hypothesis A is given by

if $\delta > 0$

$$P_{e|A} = \int_{z_2=0}^{\infty}\int_{z_1=0}^{\delta+z_2} f_{z_1|A}(z_1) f_{z_2|A}(z_2)\mathrm{d}z_1\mathrm{d}z_2$$
$$= \sum_{k_1=1}^{K_1}\sum_{k_2=K_1+1}^{K-K_1} C_{1|A}[k_1]C_{2|A}[k_2]$$
$$\left(1-\exp\left(\frac{-\delta}{\phi_A[k_1]}\right)\frac{\phi_A[k_1]}{\phi_A[k_1]+\phi_A[k_2]}\right)$$

else

$$P_{e|A} = \int_{z_2=-\delta+z_1}^{\infty}\int_{z_1=0}^{\infty} f_{z_1|A}(z_1) f_{z_2|A}(z_2)\mathrm{d}z_1\mathrm{d}z_2$$
$$= \sum_{k_1=1}^{K_1}\sum_{k_2=K_1+1}^{K-K_1} C_{1|A}[k_1]C_{2|A}[k_2]$$
$$\left(\exp\left(\frac{\delta}{\phi_A[k_2]}\right)\frac{\phi_A[k_2]}{\phi_A[k_1]+\phi_A[k_2]}\right). \quad (2)$$

The probability $P_{e|B}$ under hypothesis B can be calculated equivalently.

The pairwise error probability P_{2e} is usually used as figure of merit for binary decision problems. It is determined by the probabilities of misclassification under hypothesis A ($P_{e|A}$) and under hypothesis B ($P_{e|B}$) according to

$$P_{2e} = 0.5\left(P_{e|A} + P_{e|B}\right). \quad (3)$$

The decision threshold δ is the natural logarithm of the fraction of the determinants of the two covariance matrices given by

$$\delta = \ln\left(\frac{|\Sigma_A+\sigma^2 I|}{|\Sigma_B+\sigma^2 I|}\right) = \ln\left(\frac{|\Lambda_A|}{|\Lambda_B|}\right) = \ln\left(\frac{|\Phi_A|}{|\Phi_B|}\right),$$

where the first equation is obvious due to eigenvalue decomposition and the last equation is proven by

$$|\Phi_A| = |\Lambda_A^{0.5} U_A^H \Delta U_A \Lambda_A^{0.5}| = |\Lambda_A||\Delta|,$$
$$|\Phi_B| = |\Lambda_B^{0.5} U_B^H \Delta U_B \Lambda_B^{0.5}| = |\Lambda_B||\Delta|$$

and taking the fraction of $|\Phi_A|$ and $|\Phi_B|$.

V. Simulation Setup

This section gives an overview of the simulation setup to evaluate the performance of the presented multivariate UWB Geo-Regioning algorithm.

A. Measurement Data

The measurement data used to evaluate the performance is the same as in [1], [2], [3]. A description of the measurement campaign and arrangement of the regions can be found in [13]. The measurement parameters are listed in TABLE I for convenience.

TABLE I
PARAMETERS OF MEASUREMENT CAMPAIGN

Parameter	Value
Environment	static, indoor, industrial
Bandwidth	3 GHz
Sampling frequency	20 GHz
Region size	27 cm×56 cm
Total number of regions	22
Typical LOS regions	1 to 11 and 13, 22
Typical non-LOS regions	16 to 21

B. Alignment of CIRs

As mentioned, UWB Geo-Regioning does not require absolute timing information. Nevertheless, the measured CIRs belonging to one region must be aligned in time, such that a meaningful statistical description for the region can be extracted. Here, the CIRs are aligned to a reference sample (cf. Fig. 1) specified as their sample with the maximum absolute value. In LOS situations the CIRs are aligned to the direct path, implying that samples before the reference sample are just negligible noise samples. In case of a non-LOS situation the CIRs are aligned to the strongest path, which is not necessarily the direct path. This means that also the samples before the reference sample carry significant CIR energy. The current alignment procedure ignores these information bearing samples. This means that there is still room for improvement by using more sophisticated alignment procedures.

C. Simulation Parameters

The simulation parameters are listed in TABLE II. It can be seen from TABLE II that there are just 186 CIRs per region

TABLE II
PARAMETERS OF SIMULATION

Parameter	Value
Sampling time	0.15 ns
Reference sample	20 ($\Rightarrow$ reference time = 3 ns)
CIRs per region	620
CIRs for covariance estimation	70% ($\Rightarrow 620 \cdot 0.7 = 434$)
CIRs for algorithm testing	30% ($\Rightarrow 620 \cdot 0.3 = 186$)

available to evaluate the performance of the algorithms. To overcome this problem a method similar to *Cross Validation* [14] is used, where the performance is averaged over 50 random partitions of estimation and test data.

VI. Simulation Results

As mentioned in Section IV, the derived expressions for the probabilities of misclassification (2) hold only if all weights have a multiplicity of 1. Thus, in order to avoid numerical instabilities, too similar weights have been neglected for computing the error probabilities. Nevertheless, the analytic results match the reference results (cf. Fig. 3), calculated by Monte Carlo simulations, very well. The corresponding weights for the results in Fig. 3 are computed using an observation window of length 15 ns ($K = 100$). For the Monte Carlo simulations, 10^5 CIR realizations are drawn according to a PDF defined by the corresponding covariance matrix.

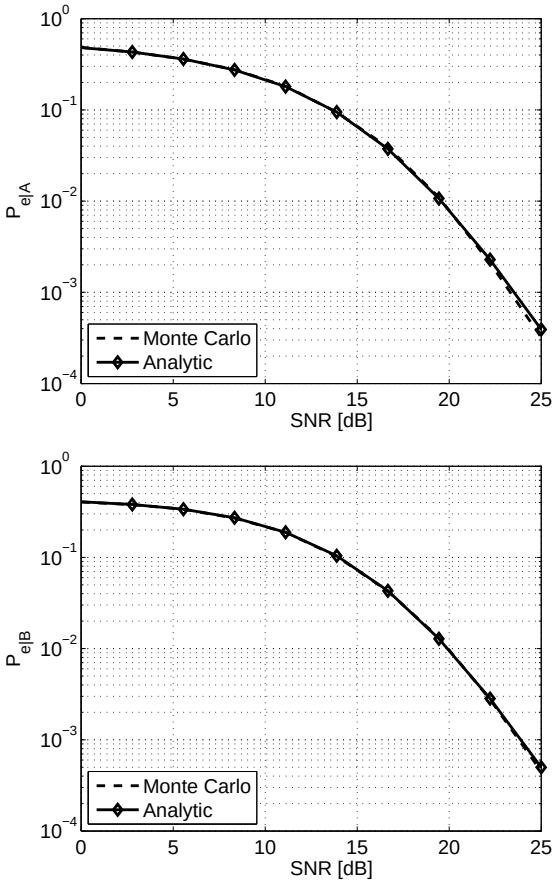

Fig. 3. Region $A = 3$ and region $B = 17$. Test CIRs distributed according to statistics of region A and B.

Fig. 4 - 7 show the performance improvement using the new covariance approach (COVARIANCE curves) instead of the previous APDP approach (APDP curves). The simulation results are obtained by averaging over 50 random partitions of estimation and test data and using an observation window of length 45 ns ($K = 300$).

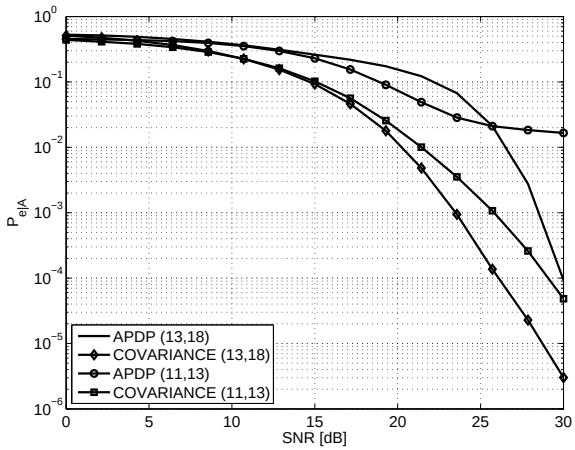

Fig. 4. Region pair (13,18): Test CIRs from region 13. Region pair (11,13): Test CIRs from region 11.

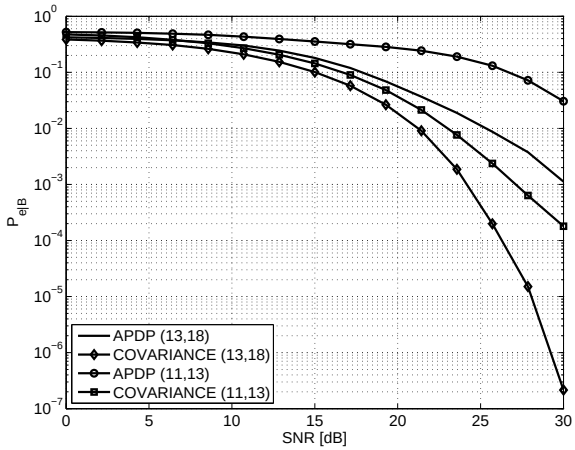

Fig. 5. Region pair (13,18): Test CIRs from region 18. Region pair (11,13): Test CIRs from region 13.

Fig. 4 and 5 depict the probabilities of misclassification ($P_{e|A}$ and $P_{e|B}$) for the two region pairs (13,18) and (11,13), where 11 and 13 are typical LOS regions and 18 is a typical non-LOS region. Deciding between 13 and 18 shows a much better performance for both approaches than deciding between 11 and 13, since the CIRs from LOS and non-LOS are very different.

Fig. 6 and 7 depict the performance curves for the region pairs (9,13) and (13,22), where all regions are LOS regions. As expected, the results deviate much less due to the more similar CIRs. Region pair (13,22) exhibits lower error probabilities for the covariance approach for both hypothesis. This is not the case for the APDP approach due to the asymmetry of the decision problem. From the curves it can be seen, that this asymmetry is not so relevant for the covariance approach, implying a more robust pairwise error probability.

From Fig. 4 it can be observed that there exists an error floor at around $P_{e|A} \approx 10^{-2} \approx 2/186$ for the APDP approach. This means that on average two out of 186 CIRs from region 11 cannot be assigned correctly to this region at

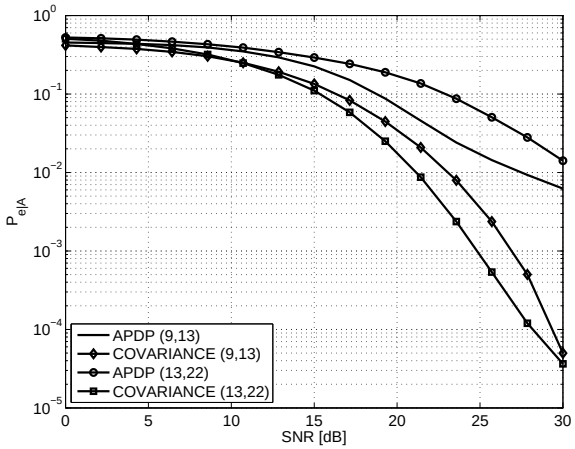

Fig. 6. Region pair (9,13): Test CIRs from region 9. Region pair (13,22): Test CIRs from region 13.

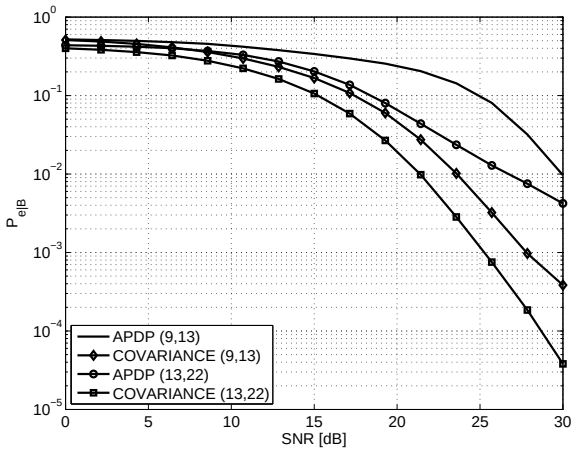

Fig. 7. Region pair (9,13): Test CIRs from region 13. Region pair (13,22): Test CIRs from region 22.

high SNR. Similar error floors for the APDP performance are visible at high SNRs for several other regions pairs. Using the covariance algorithm, these error floors can be removed. This fact suggests that the covariance model describes reality better than the APDP model, which ignores correlations between CIR taps. Another consequence is that the uncorrelated scattering assumption for different path delays, often used for statistical channel models, doesn't hold for the considered measurement data.

The covariance approach shows significant SNR gains visible in Fig. 4 - 7 (up to 10 dB in Fig. 6). These gains are vital for UWB communication systems, which work generally in the low SNR regime due to transmit power restrictions. In order to achieve a pairwise error probability of 10^{-2}, an SNR in the range of 20 to 25 dB is necessary even for the covariance approach, which is still very high for UWB technology. Fortunately, a higher SNR can be expected for channel estimation compared to data detection by using a noise averaging method.

VII. Conclusions

In this work we have introduced a new statistical model to describe geographic regions accounting also for tap correlations of CIRs. We have derived the respective multivariate maximum likelihood decision algorithm and provided an analytic expression for the probabilities of misclassification. The simulation results showed the performance improvement achieved by the new modeling approach. The trade-off is increased receiver complexity, since it must estimate the full CIR for the covariance approach including magnitude and phase compared to magnitude-only-estimation for the APDP approach.

In future work, the performance of UWB Geo-Regioning will be investigated in mobile environments, where the coherence time of the channel forces adaptation of the a-priori statistics for the regions. Presumably, a new statistical model for geographic regions accounting for time and frequency dispersiveness, or frequent a-priori statistics updates will be necessary.

VIII. Acknowledgements

The authors would like to thank all partners of the project PULSERS II, that is partially funded by the European Commission and the Swiss Federal Office for Education and Science, for their contributions and constructive discussions.

References

[1] F. Althaus, F. Troesch, and A. Wittneben, "UWB geo-regioning in rich multipath environment," in *IEEE Vehicular Technology Conference*, Dallas, USA, Sept. 2005, pp. 1001–1005.

[2] ——, "Geo-regioning in UWB networks," in *14th IST Mobile and Wireless Communications Summit*, Dresden, Germany, June 2005.

[3] C. Steiner, F. Althaus, and A. Wittneben, "On the performance of UWB geo-regioning," in *The Seventh IEEE International Workshop on Signal Processing Advances in Wireless Communications*, Cannes, France, July 2006, p. 5.

[4] D. Porcino and W. Hirt, "Ultra-wideband radio technology: Potential and challenges ahead," *IEEE Communications Magazine*, vol. 41, no. 7, pp. 66–74, July 2003.

[5] S. Gezici, Z. Tian, G. Giannakis, H. Kobayashi, A. Molisch, H. Poor, and Z. Sahinoglu, "Localization via ultra-wideband radios," *IEEE Signal Processing Magazine*, vol. 22, no. 4, pp. 70–84, July 2005.

[6] B. Denis, J. Keignart, and N. Daniele, "Impact of NLOS propagation upon ranging precision in UWB systems," in *IEEE Conference on Ultra Wideband Systems and Technologies*, Reston, USA, Nov. 2003, pp. 379 – 383.

[7] Y. Qi, H. SUda, and H. Kobayashi, "On time-of-arrival positioning in a multipath environment," in *IEEE Vehicular Technology Conference*, Los Angeles, USA, Sept. 2004, pp. 3540–3544.

[8] J.-Y. Lee and R. A. Scholtz, "Ranging in a dense multipath environment using an UWB radio link," *IEEE Journal on Selected Areas in Communications*, vol. 20, no. 9, pp. 1677–1683, Dec. 2002.

[9] T. Anderson, *An Introduction to Multivariate Statistical Analysis*, 3rd ed. John Wiley and Sons, Inc., 2003.

[10] M. Schwartz, *Communication Systems and Techniques*, 1st ed. McGraw-Hill, 1966.

[11] J. G. Proakis, *Digital Communications*, 4th ed. McGraw-Hill, 2001.

[12] H. V. Khuong and H.-Y. Kong, "General expression for pdf of a sum of independent exponential random variables," *IEEE Communications Letters*, vol. 10, no. 3, pp. 159–161, Mar. 2006.

[13] F. Althaus, F. Troesch, T. Zasowski, and A. Wittneben, "STS measurements and characterization," *PULSERS Deliverable D3b6a*, vol. IST-2001-32710 PULSERS, 2005.

[14] C. M. Bishop, *Neural Networks for Pattern Recognition*, 1st ed. Clarendon Press, Oxford, 1995.